



THE UNIVERSITY *of* EDINBURGH

Edinburgh Research Explorer

Flutriciclamide (18F-GE180) PET

Citation for published version:

Fan, Z, Calsolaro, V, Atkinson, RÁ, Femminella, GD, Waldman, A, Buckley, C, Trigg, W, Brooks, DJ, Hinz, R & Edison, P 2016, 'Flutriciclamide (18F-GE180) PET: first in human PET study of novel 3rd generation in vivo marker of human translator protein' *Journal of Nuclear Medicine*. DOI: 10.2967/jnumed.115.169078

Digital Object Identifier (DOI):

[10.2967/jnumed.115.169078](https://doi.org/10.2967/jnumed.115.169078)

Link:

[Link to publication record in Edinburgh Research Explorer](#)

Document Version:

Peer reviewed version

Published In:

Journal of Nuclear Medicine

Publisher Rights Statement:

This research was originally published in JNM. Zhen Fan*,1, Valeria Calsolaro*,1, Rebecca A. Atkinson1, Grazia D. Femminella1, Adam Waldman1, Christopher Buckley2, William Trigg2, David J. Brooks1,3, Rainer Hinz4 and Paul Edison. Flutriciclamide (18F-GE180) PET: First-in-Human PET Study of Novel Third-Generation In Vivo Marker of Human Translocator Protein . JNM. 2016;vol 57:1753-1759 . © by the Society of Nuclear Medicine and Molecular Imaging, Inc.

General rights

Copyright for the publications made accessible via the Edinburgh Research Explorer is retained by the author(s) and / or other copyright owners and it is a condition of accessing these publications that users recognise and abide by the legal requirements associated with these rights.

Take down policy

The University of Edinburgh has made every reasonable effort to ensure that Edinburgh Research Explorer content complies with UK legislation. If you believe that the public display of this file breaches copyright please contact openaccess@ed.ac.uk providing details, and we will remove access to the work immediately and investigate your claim.



Flutriciclamide (^{18}F -GE180) PET: first in human PET study of novel 3rd generation in vivo marker of human translator protein.

Running title: ^{18}F -GE180 PET

Zhen Fan^{1*}, Valeria Calsolaro^{1*}, Rebecca A. Atkinson¹, Grazia D. Femminella¹, Adam Waldman¹, Christopher Buckley², William Trigg², David J. Brooks^{1, 3}, Rainer Hinz R⁴, Paul Edison¹

1 - Neurology Imaging Unit, Imperial College London, Hammersmith Hospital, London, W120NN, UK.

2 - GE Healthcare, Grove Centre, Amersham, UK

3 - Institute of Clinical Medicine, Aarhus University, Denmark

4 - Wolfson Molecular Imaging Centre, University of Manchester, UK

Corresponding author:

Dr Paul Edison MBBS, MRCP, PhD, FRCPI

Neurology Imaging Unit,

Imperial College London,

Hammersmith Hospital Campus,

London, W12 0NN, UK.

Tel: +44(0)20 3313 3725 Fax: +44(0)20 8383 1783

Email: paul.edison@imperial.ac.uk

First Author

Zhen Fan MSc (PhD student) and Valeria Calsolaro MD (Fellow)

NIU, Imperial College London,

Hammersmith Hospital Campus,

London,

W12 0NN, UK.

Tel: +44(0)20 3313 3725 Fax: +44(0)20 8383 1783

Email: zhen.fan10@imperial.ac.uk and v.calsolaro@imperial.ac.uk

Word count: 4984

Financial Support: Alzheimer's Research UK, GE Healthcare, National Institute for Health Research.

* Both authors contributed equally to the paper

ABSTRACT

Neuroinflammation is associated with neurodegenerative disease. PET (positron emission tomography) radioligands targeting the 18 kDa translocator protein (TSPO) has been used as in vivo markers of neuroinflammation, but there is an urgent need for novel probes with improved signal-to-noise ratio. Flutriciclamide (^{18}F -GE180) is a recently developed third generation TSPO ligand. In this first study, we evaluated the optimum scan duration and kinetic modelling strategies for ^{18}F -GE180 PET in (older) healthy controls (HC).

Methods: Ten HC, six TSPO high affinity binders (HABs) and four mixed affinity binders (MABs), were recruited. All subjects had detailed neuropsychological tests, MRI and a 210 min ^{18}F -GE180 dynamic PET/CT scan using metabolite corrected arterial plasma input function. We evaluated five different kinetic models: irreversible and reversible two-tissue compartment models, a reversible one-tissue model and two models with an extra irreversible vascular compartment. The optimum scan length was investigated based on 210 min scan data. The feasibility of generating parametric maps was also investigated using graphical analysis.

Results: ^{18}F -GE180 concentration was higher in plasma than in whole blood during the entire scan duration. Using the kinetic model, the volume of distribution (V_T) was 0.17 in HABs and 0.12 in MABs. The model that best represented brain ^{18}F -GE180 kinetics across regions was the reversible two-tissue compartment model (2TCM4k) and 90 min resulted as the optimum scan length required to obtain stable estimates. Logan graphical analysis with arterial input function gave a V_T highly consistent with V_T in kinetic model, which could be used for voxel-wise analysis.

Conclusion: We report for the first time the kinetic properties of the novel third generation TSPO PET ligand, ^{18}F -GE180, in humans: 2TCM4k is the optimal method to quantify the brain uptake, 90 min is the optimal scan length and Logan approach could be used to generate parametric maps. While these control subjects have shown relatively low V_T , the methodology presented here forms the basis for quantification for future PET studies using ^{18}F -GE180 in different pathologies.

Key words: GE180, Flutriciclamide, Kinetic Model, Logan analysis, PET.

INTRODUCTION

Microglia plays a crucial role as the first line of defense when neuronal damage occurs. Under normal conditions microglial cells are in a state of surveillance with elongated processes. During injury or neurodegenerative processes, microglial cells become activated; the activated state is mirrored by up regulation of translocator protein (TSPO) (1, 2). Positron emission tomography (PET) with TSPO specific ligands provide an in vivo technique to detect microglial activation (3).

¹¹C-(R)-PK11195 PET has been used for more than two decades. However, due to low signal-to-background ratio and short half-life (20 min), second generation TSPO markers have been developed. These include ¹⁸F-FEPPA, ¹⁸F-FEDAA1106, ¹¹C-vinpocetine, ¹¹C-DAC, ¹¹C-DAA1106, ¹¹C-N1-methyl-2-phenylindol-3-ylglyoxylamide, ¹¹C-CLINME, ¹¹C-DPA-713, ¹⁸F-DPA-714, ¹⁸F-PBR06 and ¹¹C-PBR28 (4). However, the results obtained by second generation radioligands in pre-clinical models have not been consistently reproduced in humans (5). Their quantification in humans suffers from three confounding factors (6). The first factor is genetic: a single nucleotide polymorphism in the TSPO gene (rs6971) leads to an amino-acid substitution (A147T) and reduced binding affinity. The second factor is the disproportion between the high signal from the TSPO in the endothelial cells of the blood-brain barrier (BBB) and venous sinuses and the signal from the tissue, requiring appropriate kinetic correction (7). The third factor is the difficulty in obtaining accurate estimates of free plasma concentrations for proper quantification.

Flutriciclamide (^{18}F -GE180) has been identified as a promising TSPO tracer in preclinical models of stroke and lipopolysaccharide (LPS)-induced central nervous system inflammation (8, 9). Here we report the results of a study evaluating ^{18}F -GE180 PET in healthy human brains. We have investigated: 1) blood tracer concentrations 2) brain uptake 3) quantification of binding via tracer kinetic modeling 4) optimal scan length and 5) feasibility of generating parametric maps.

MATERIALS AND METHODS

Fifteen HC aged 50-85 were recruited. Subjects who were high (HABs=6) or mixed affinity binders (MABs=4) proceeded to MRI and PET scans, while low affinity binders (LABs=5) were excluded. Details of recruitment, demography, and MRI acquisition in Supplementary file 1.

GE180 PET

^{18}F -GE180 was manufactured on the GE FASTlab (10). All subjects received 185 MBq ^{18}F -GE180 by bolus intravenous injection (in 20 seconds) immediately before the PET scan. The scan was acquired using a Siemens Biograph 6 PET/CT scanner (11). An initial CT was acquired for patient position and for attenuation correction of PET images. The tracer was then injected and dynamic emission PET images were acquired over 210 minutes using predetermined time frames: 6x15s, 3x60s, 5x120s, 5x300s, and 14x600s. Images were corrected for attenuation, random and scattered emissions based on the 3D ordinary Poisson ordered-subset expectation maximization algorithm. Reconstruction of PET was carried out using filtered back projection.

Blood data

Arterial whole blood activity was continuously monitored for the first 15 min of the PET scan using the Allogg automated blood sampling system (ABSS) with real-time online blood sampling. Ten discrete arterial blood samples were taken at 5, 10, 15, 30, 60, 90, 120, 150, 180 and 210 min of the PET scan. The activity concentration was measured in both whole blood and plasma by a well counter and was used to generate a plasma: blood ratio curve. Applying the plasma: blood ratio model to the first 15 min of continuous whole blood data, the time course of activity in the plasma can be estimated with a sigmoidal fitting.

Metabolites of ^{18}F -GE180 were measured by HPLC (High-performance liquid chromatography) analysis (10) using discrete blood samples. A two-exponential linear model was used to describe the parent fraction of ^{18}F -GE180, which was applied to the plasma to generate the parent plasma input function. Standardized uptake value (SUV) was applied to both total blood and parent plasma with the formula:

$$SUV = \frac{^{18}\text{F} - \text{GE180 activity concentration}(kBq/ml)}{^{18}\text{F} - \text{GE180 injected dose}(MBq) / \text{Body Weight}(kg)}$$

Finally, the time delay (the arrival of the ^{18}F -GE180 bolus at the peripheral sampling site) was determined using MICK.exe (Quantitative software for the PET analysis) and were performed based on MATLAB®2014 (The MathWorks, USA) on Windows platform.

Region of interest analysis

Each subject underwent two 90 min PET scans with a 20 min break in between; the realignment approach was necessary to re-align the second scan to the first scan. Head motions were corrected using the frame-by-frame realignment tools in Statistical

Parametric Mapping (SPM). Based on the visual resolution, the 8th frame (185–245s) was selected as the reference frame for each time frame realigning to. An individualized object map in PET space was created with the following procedure: 1) MRI was co-registered to the PET add image (60 – 90 min); 2) a binary grey and white matter mask was created via segmentation; 3) the probabilistic ROI atlas (12) in MNI space was transformed into native PET space; 4) we applied the binary mask to the ROI atlas to generate individual ROIs. Regional time activity curves (TACs) were generated by sampling the dynamic PET images with the individual ROIs for the following merging regions: frontal, temporal, parietal, occipital lobes and whole brain. Additional sampling of posterior cingulate, thalamus, brainstem, whole medial temporal lobe, hippocampus, and cerebellum was performed. The parahippocampus, anterior cingulate and amygdala were sampled as additional ROIs using Analyze 11.0. The SUV TAC was generated for each ¹⁸F-GE180 dynamic PET by dividing the ratio of ¹⁸F-GE180 injected dose over body weight.

Kinetic modeling

Parent plasma input function and dynamic PET were used to investigate the best kinetic model to compute ¹⁸F-GE180 total volume of distribution (V_T) from TACs using MICK software (Modeling-Input-function-Compartmental-Kinetics) and MATLAB. We evaluated five different kinetic models (Supplementary file 2). ¹⁸F-GE180 tissue data were investigated with the reversible one-tissue 2k (1TCM2k), the two-tissue 4k (2TCM4k) model and the irreversible two-tissue 3k (1TCM3k), where k implies the rate constant for tracer for different kinetic compartments. As tracer binds to BBB endothelial cells, endothelia could have significant impact on kinetic modeling (13, 14); therefore we also considered one-tissue with extra vascular component (1TCM2k-1k) and two-tissue with

extra vascular component (2TCM4k-1k). The additional component describes the trapping of the tracer by the endothelial cells of blood vessels. Akaike Information Criterion (AIC) (15) is a statistical measure to estimate the quality of fit of the predicted model against the actual data using different statistical models. In simple terms, the AIC values indicate the information lost when a candidate model is applied to estimate the real data, and the model with the smallest AIC value should be selected as the preferred model, as it indicates the best fit (16). In order to select the best model to quantify the tracer, AIC is calculated using the following formula:

$$AIC = n * \ln(wrss) + 2m$$

where m denotes number of parameters, n equals the sum of degrees of freedom and number of parameters, wrss denotes weighted residual sum of squares (17). The AIC fraction was also calculated by measuring the frequency of AIC preferences for each model across all subjects (18). AIC was calculated for the following brain regions: frontal, temporal, parietal, occipital lobes, whole brain, posterior-cingulate, thalamus, striatum, brainstem, medial-temporal-lobe, hippocampus and cerebellum. Coefficient of variation (CV) was measured to assess dispersion and precision of parameters. We also evaluated the separation in average binding between high and mixed affinity binder classes.

Graphical analysis

Graphical analysis was applied to investigate the feasibility of generating parametric maps of ¹⁸F-GE180. Logan or Patlak plot were involved based on the nature of the tracer (reversible or irreversible). Initially we calculated the optimal threshold time by linear fit the tissue:plasma ratio against the time. ¹⁸F-GE180 parametric maps were generated with

the parent plasma input function and dynamic PET images using MICK parametric map software on MATLAB.

Optimisation of scan length

The optimum scan duration was evaluated measuring the percentage change of k (rate constants) and V_T , along with their CV at different time durations, calculated at 60 min, 75 min, 90 min, 150 min, 180 min, and 210 min. k_3 and k_4 indicate the rate constant of ^{18}F -GE180 in and out of the specific-bound compartment, while the k_3/k_4 ratio represents the specific binding of the tracer. Thus, the k_3/k_4 ratio was measured to investigate whether the binding potential of ^{18}F -GE180 was affected when the scanning time was reduced.

Statistical analysis

Statistical analysis of group-wise differences between different kinetic models, different scan durations and ROI V_T in different genetic groups was calculated in SPSS for Windows version 22 (SPSS, Chicago, Illinois, USA). A p value of <0.05 was regarded as a statistical difference. The Pearson correlation was applied to measure the linear correlation between two groups of variables using SPSS22. Repeated measures ANOVA (analysis of variance) was applied to detect any overall differences between repeated measurements.

RESULTS

Parent plasma input

Consistent with the preclinical work (8), the radiochromatogram revealed three identifiable radiolabeled metabolites and a parent ^{18}F -GE180 in human plasma (Fig.1A). The parent fraction of ^{18}F -GE180 gradually reduced from 90% to 60%. There was no group difference

between HABs and MABs in metabolic rates and plasma: blood curve (Fig.1B and Fig.1C). The ^{18}F -GE180 activity concentration in plasma was 1.6-fold higher than in whole blood. No difference in parent plasma input function between HABs and MABs was found (Fig.1D).

Dynamic PET image TAC

As tracer concentrations are correlated with injected dose and individual weight, we measured SUV TAC values at each time frame. The tracer activity concentration in the brain peaked at 125 seconds with SUV at 1.5 and then quickly washed out and reached a plateau around 40 min. As a group, SUVs were significantly higher in HABs than MABs in temporal lobe ($p=0.0001$), thalamus ($p=0.0001$) and striatum ($p=0.0002$) (Fig.2). The venous sinuses showed consistently highest tracer activity throughout the scan, while grey matter showed around 30% higher activity concentration than white matter.

Kinetic modeling

Among five kinetic models, two-tissue reversible model (2TCM4k) showed the lowest AIC value in frontal (-59.6 ± 5.4), temporal (-46.4 ± 4.5), parietal (-58.6 ± 5.4) and occipital lobes (-54.3 ± 5.1) as a group (Fig 3A). 2TCM4k model also showed the highest AIC fraction (Fig 3B). While the 2TCM3k irreversible model demonstrated closer AIC values (less than 10% difference compared to 2TCM4k model), the k_i (net influx constant), demonstrating the overall net rate of tracer uptake into tissue in 2TCM3k model, showed poor precision with high coefficient of variation ($CV=104\pm 85\%$) while V_T in reversible 2TCM4k had a CV of $21\pm 13\%$. Based on the model curve fitting, 2TCM4k provided a good fit to ^{18}F -GE180 activity, supported by smallest weighted residual sum square and more random in residual's sequence (similar number of residuals above or below the model curve) using

Wald-Wolfowitz test. In summary, the 2TCM4k is the preferred method of analysis of ^{18}F -GE180 PET. Supplementary file 3 details rate constants (K_1 , k_2 , k_3 and k_4), blood volume and V_T applying the 2TCM4k model in HABs and MABs which showed good precision of parameter estimation.

Volume of distribution

As a group, ten HC had low mean V_T in whole brain, but slightly higher in temporal lobe, occipital lobe and thalamus (Fig.4). Thalamus, parahippocampus, and cerebellum showed significantly higher mean V_T values in HABs compared with MABs (Table 1).

Scan length

210 min data was excluded as variance was very high towards the end of the scan. Repeated ANOVA did not show difference in the absolute V_T when reducing the scan duration. In this study, the group mean of k_3/k_4 ratio (HAB=0.52 and MAB=0.34) was calculated to evaluate the results among different scan lengths, showing no differences with scan length reduction from 180 min to 90 min. When the scan length was further reduced to 75 min, the k_3/k_4 ratio remained the same as with the 90 min data, but four individual subjects showed a 14% reduction in k_3/k_4 ratio. Compared to 90 min scans, 60 min scans showed a 51% reduction in k_3/k_4 ratio as a group. These data suggest that for this cohort the optimal scan duration is 90 min.

LOGAN

Kinetic modelling suggested that ^{18}F -GE180 has a reversible feature, therefore we applied Logan graphical analysis (19) to generate parametric maps. Based on linear fit of the whole brain and the appropriate weight for different time points, dynamic data from 20 to 90 min

(8 data points) were selected to generate Logan straight line (slope= 0.147 ± 0.06 and intercept= -1623 ± 387) for parametric map (Fig.5). The Logan V_T values (Supplementary file 4) were correlated with 2TCM4k V_T values with a strong correlation in four cortices and hippocampus in both HABs ($p<0.0001$) and MABs ($p<0.0001$) (Fig. 6). The HABs showed generally higher Logan V_T values than MABs; however, there were no statistically significant differences in this small sample.

DISCUSSION

This is the first study evaluating different approaches for PET modelling of the third generation TSPO tracer ^{18}F -GE180 in older healthy subjects, establishing the optimum scanning time in this study population. There was consistently higher ^{18}F -GE180 activity in plasma than in whole blood, but brain V_T values generated from plasma input functions were low (around 0.16). Data were acquired for 210 min after injection of ^{18}F -GE180 and five different kinetic models were evaluated in this study. The ^{18}F -GE180 V_T remained unchanged when the scan length was reduced to 90 min, but changes were observed when reducing the scan length to 75 min and 60 min, suggesting that 90 min might be the minimal scan time for ^{18}F -GE180 PET. The 2TCM4k model demonstrated the lowest AIC and CV among the five kinetic models, suggesting that the 2TCM4k model could be the best model to estimate ^{18}F -GE180 uptake. Compared to the 2TCM4k model, Logan graphical analysis allows us to create parametric maps and to estimate V_T at voxel level. Logan V_T was highly correlated with 2TCM4k V_T in all cortices, indicating that the Logan graphical analysis can be used to create unbiased parametric V_T maps for ^{18}F -GE180.

Consistent with a preclinical study (8), HPLC revealed three separate ^{18}F -GE180 plasma metabolites, with a similar profile in HAB and MAB and no significant differences between HABs and MABs in plasma: blood ratios. The plasma: blood ratio for tracers crossing the BBB by passive diffusion is close to unity at the beginning of PET. ^{18}F -GE180 showed a relatively high plasma: blood ratio of 1.55, indicating higher concentration in plasma over red blood cells. A persistently high plasma: blood ratio throughout the scan reflects poor membrane penetration of ^{18}F -GE180 across red cell membranes. In vitro assays of plasma protein binding of ^{18}F -GE180 in human samples showed a relatively high percentage (97.4%) plasma protein binding, which was also seen with other TSPO tracers.

Preclinical animal models showed that ^{18}F -GE180 crosses the BBB readily. In humans, ^{18}F -GE180 demonstrated a relatively low V_T in the brain, possibly due to: 1) low availability of the GE180 due to significant plasma protein binding, 2) low BBB permeability or 3) clearance by efflux pumps. Despite the fact that species differences have been observed in the BBB structure (20) and other novel brain PET tracers (21), the significant difference observed between human and preclinical models in ^{18}F -GE180 could be primarily due to a significantly higher binding to plasma protein in humans.

^{18}F -GE180 preclinical studies demonstrated that, in rats, there is a clear regional differentiation of high TSPO expressing regions (olfactory bulbs) compared to low TSPO expressing regions (striatum) (22). In this study, five subjects (1 MAB and 4 HABs) revealed lowest uptake in striatum, three (MABs) showed lowest uptake in cerebellum, two (HABs) showed a more generalized distribution of TSPO expression. This inconsistent

pattern suggests that a single predefined reference region for non-specific binding may not be appropriate for ^{18}F -GE180 in humans in this age group.

As TSPO expression is low in healthy brain, the ^{18}F -GE180 V_T values were relatively small in all ROI regions (range 0.15 to 0.20). A higher signal in thalamus compared to other regions was found, consistent with previous ^{11}C -(R)-PK11195 studies (23). However, V_T values of ^{18}F -GE180 suggest that tracer brain uptake is relatively low compared to other TSPO PET radioligands, though the impact of this radioligand as a microglial imaging marker cannot be determined until we have results in specific disease conditions. The significant inverse correlation between the ^{18}F -GE180 input function and the V_T in brain suggests reflects the higher uptake to plasma proteins in humans compared to animal models.

Interestingly, the significant inverse correlation between ^{18}F -GE180 input function and V_T in brain for each binding class separately, with a correlation coefficient > 0.9 , indicates that whole brain V_T can be almost entirely predicted by plasma levels within each binding class. Given that it was not possible to estimate plasma free fractions reliably, possibly because the fluctuations in estimated V_T may be due to fluctuations in free fractions across subjects. Indeed, higher plasma protein binding would result in higher plasma counts and lower volume of distribution. This observation replicates similar observations in other TSPO tracers (13, 24). Identification of an optimal reference method would allow us to further refine the analysis methods without the arterial input.

Most 2nd generation TSPO tracers, such as ¹¹C-PBR28 and ¹¹C-PBR111, demonstrated an association with the TSPO genotype, revealing a 30% higher uptake in whole brain of HABs than MABs. In this study, there was a 30-40% higher uptake in HABs, reaching significance in thalamus, parahippocampus and cerebellum. Nevertheless, there was some overlap between subjects; moreover their numbers in the study were also small. Compared to some second generation TSPO tracers, ¹⁸F-GE180 may be less sensitive to the TSPO binding affinity status and may behave more like ¹¹C-(R)-PK11195. One could argue, some of the variability seen in the MABs and HABs could be due to test-retest variability, which we are evaluating. The high correlation between Logan V_T and 2TCM4k V_T suggests that Logan parametric mapping could be used to generate pixel-wise parametric V_T maps. As Logan generally underestimates the V_T (25), there was no statistically significant difference between HAB and MAB, potentially due to the small numbers in this pilot study. Additionally, consistently with V_T results, the Logan V_T parametric maps demonstrated heterogeneous distribution of ¹⁸F-GE180 uptake in the HC. This heterogeneity was observed in both HAB and MAB subgroups and was consistent with 2TCM4k model.

While one of the limitations of this study is the small sample size, this pilot study provides the first insight into the performance of ¹⁸F-GE180 in normal human brain and information about the parent plasma input function. Another limitation is the exclusion of the LAB from the study, and our laboratory is recruiting more participants to evaluate this tracer further. The low expression of TSPO in normal brain could be another limitation of this study evaluating only HC. However, these scans were performed with an arterial input

function and an extensive scanning time of 210 min, providing significant information about the tracer kinetics and modelling of this novel TSPO tracer for future use.

CONCLUSION

This pilot study provides preliminary brain uptake kinetics of the novel TSPO tracer ^{18}F -GE180 in HC. We have demonstrated for the first time that ^{18}F -GE180 shows uptake into the brain of HC and that the tracer V_T could be effectively modelled using a 2TCM4k and Logan graphical models to quantify the TSPO binding in human brain. The plasma: blood ratio and the rate of metabolism and input functions were not different between HAB and MAB subjects. We have also demonstrated that 90 min is the optimal scan duration, providing enough information to generate the precise and accurate estimates of V_T . Semi-quantitative SUV analysis for tracer uptake demonstrated a good correlation with kinetic modeling V_T values. Logan graphical analysis with arterial input function enables us to generate ^{18}F -GE180 parametric maps for voxel-wise analyses.

DISCLOSURE

Dr. Edison is funded by Higher Education Funding Council for England and received grants from Alzheimer's Research, UK, Alzheimer's Drug Discovery Foundation, Alzheimer's Society, UK, Novo Nordisk, Piramal Life Science and GE Healthcare.

Calsolaro Valeria is funded by the Alzheimer's Research UK fellowship.

Dr. Trigg and Dr. Buckley are funded by GE Healthcare.

Prof. Brooks has received research grants from the Medical Research Council, Alzheimer's Research Trust, during the conduct of the study; other from GE Healthcare, personal fees

from AstraZeneca, Cytos, Shire, Novartis, GSK (Holland), Navidea, UCB, and Acadia, grants from Michael J Fox Foundation, European Commission, outside the submitted work. Miss Zhen Fan, Miss Rebecca A. Atkinson, Dr. Grazia D. Femminella, Dr Adam Waldman, and Dr. Rainer Hinz have nothing to declare.

ACKNOWLEDGEMENTS

We thank GE Healthcare for providing the radiotracers, Imperial College Clinical Imaging Facility for providing MRI and PET imaging facilities. We thank Dr Albert Busza, Andy Blyth, Stephanie McDevitt, Neva Patel and Gokul Kolipaka for ^{18}F -GE180 scanning.

REFERENCES

1. Lavis S, Guillemier M, Herard AS, et al. Reactive astrocytes overexpress TSPO and are detected by TSPO positron emission tomography imaging. *J Neurosci*. 2012;32:10809-10818.
2. Gatliff J, Campanella M. TSPO: kaleidoscopic 18-kDa amid biochemical pharmacology, control and targeting of mitochondria. *Biochem J*. 2016;473:107-121.
3. Ching AS, Kuhnast B, Damont A, Roeda D, Tavitian B, Dolle F. Current paradigm of the 18-kDa translocator protein (TSPO) as a molecular target for PET imaging in neuroinflammation and neurodegenerative diseases. *Insights Imaging*. 2012;3:111-119.
4. Chauveau F, Boutin H, Van Camp N, Dolle F, Tavitian B. Nuclear imaging of neuroinflammation: a comprehensive review of [11C]PK11195 challengers. *Eur J Nucl Med Mol Imaging*. 2008;35:2304-2319.
5. Rahmim A, Qi J, Sossi V. Resolution modeling in PET imaging: theory, practice, benefits, and pitfalls. *Med Phys*. 2013;40:064301.
6. Turkheimer FE, Rizzo G, Bloomfield PS, et al. The methodology of TSPO imaging with positron emission tomography. *Biochemical Society Transactions*. 2015;43:586-592.
7. Rizzo G, Veronese M, Tonietto M, Zanotti-Fregonara P, Turkheimer FE, Bertoldo A. Kinetic modeling without accounting for the vascular component impairs the quantification of [(11)C]PBR28 brain PET data. *J Cereb Blood Flow Metab*. 2014;34:1060-1069.
8. Boutin H, Murray K, Pradillo J, et al. 18F-GE-180: a novel TSPO radiotracer compared to 11C-R-PK11195 in a preclinical model of stroke. *Eur J Nucl Med Mol Imaging*. 2015;42:503-511.
9. Dickens AM, Vainio S, Marjamaki P, et al. Detection of microglial activation in an acute model of neuroinflammation using PET and radiotracers 11C-(R)-PK11195 and 18F-GE-180. *J Nucl Med*. 2014;55:466-472.
10. Wickstrom T, Clarke A, Gausemel I, et al. The development of an automated and GMP compliant FASTlab Synthesis of [(18) F]GE-180; a radiotracer for imaging translocator protein (TSPO). *J Labelled Comp Radiopharm*. 2014;57:42-48.
11. Poon JK, Dahlbom ML, Casey ME, Qi J, Cherry SR, Badawi RD. Validation of the SimSET simulation package for modeling the Siemens Biograph mCT PET scanner. *Phys Med Biol*. 2015;60:N35-N45.

12. Hammers A, Chen CH, Lemieux L, et al. Statistical neuroanatomy of the human inferior frontal gyrus and probabilistic atlas in a standard stereotaxic space. *Hum Brain Mapp.* 2007;28:34-48.
13. Guo Q, Owen DR, Rabiner EA, Turkheimer FE, Gunn RN. Identifying improved TSPO PET imaging probes through biomathematics: the impact of multiple TSPO binding sites in vivo. *Neuroimage.* 2012;60:902-910.
14. Rizzo G, Veronese M, Tonietto M, Zanotti-Fregonara P, Turkheimer FE, Bertoldo A. Kinetic modeling without accounting for the vascular component impairs the quantification of [C-11]PBR28 brain PET data. *Journal of Cerebral Blood Flow and Metabolism.* 2014;34:1060-1069.
15. Aho K, Derryberry D, Peterson T. Model selection for ecologists: the worldviews of AIC and BIC. *Ecology.* 2014;95:631-636.
16. Akaike H. Information theory and an extension of the maximum likelihood principle. *Selected Papers of Hirotugu Akaike*: Springer; 1998:199-213.
17. Turkheimer FE, Hinz R, Cunningham VJ. On the undecidability among kinetic models: From model selection to model averaging. *Journal of Cerebral Blood Flow and Metabolism.* 2003;23:490-498.
18. Mansor S, Boellaard R, Froklage FE, et al. Quantification of Dynamic 11C-Phenytin PET Studies. *J Nucl Med.* 2015;56:1372-1377.
19. Logan J. Graphical analysis of PET data applied to reversible and irreversible tracers. *Nuclear Medicine and Biology.* 2000;27:661-670.
20. Syvanen S, Lindhe O, Palner M, et al. Species Differences in Blood-Brain Barrier Transport of Three Positron Emission Tomography Radioligands with Emphasis on P-Glycoprotein Transport. *Drug Metabolism and Disposition.* 2009;37:635-643.
21. Alstrup AK, Landau AM, Holden JE, et al. Effects of anesthesia and species on the uptake or binding of radioligands in vivo in the Gottingen minipig. *Biomed Res Int.* 2013;2013:808713-808719.
22. Wadsworth H, Jones PA, Chau WF, et al. [(1)(8)F]GE-180: a novel fluorine-18 labelled PET tracer for imaging Translocator protein 18 kDa (TSPO). *Bioorg Med Chem Lett.* 2012;22:1308-1313.
23. Doble A, Malgouris C, Daniel M, et al. Labelling of peripheral-type benzodiazepine binding sites in human brain with [3H]PK 11195: anatomical and subcellular distribution. *Brain Res Bull.* 1987;18:49-61.

- 24.** Endres CJ, Pomper MG, James M, et al. Initial evaluation of ¹¹C-DPA-713, a novel TSPO PET ligand, in humans. *J Nucl Med.* 2009;50:1276-1282.
- 25.** Slifstein M, Laruelle M. Effects of statistical noise on graphic analysis of PET neuroreceptor studies. *J Nucl Med.* 2000;41:2083-2088.

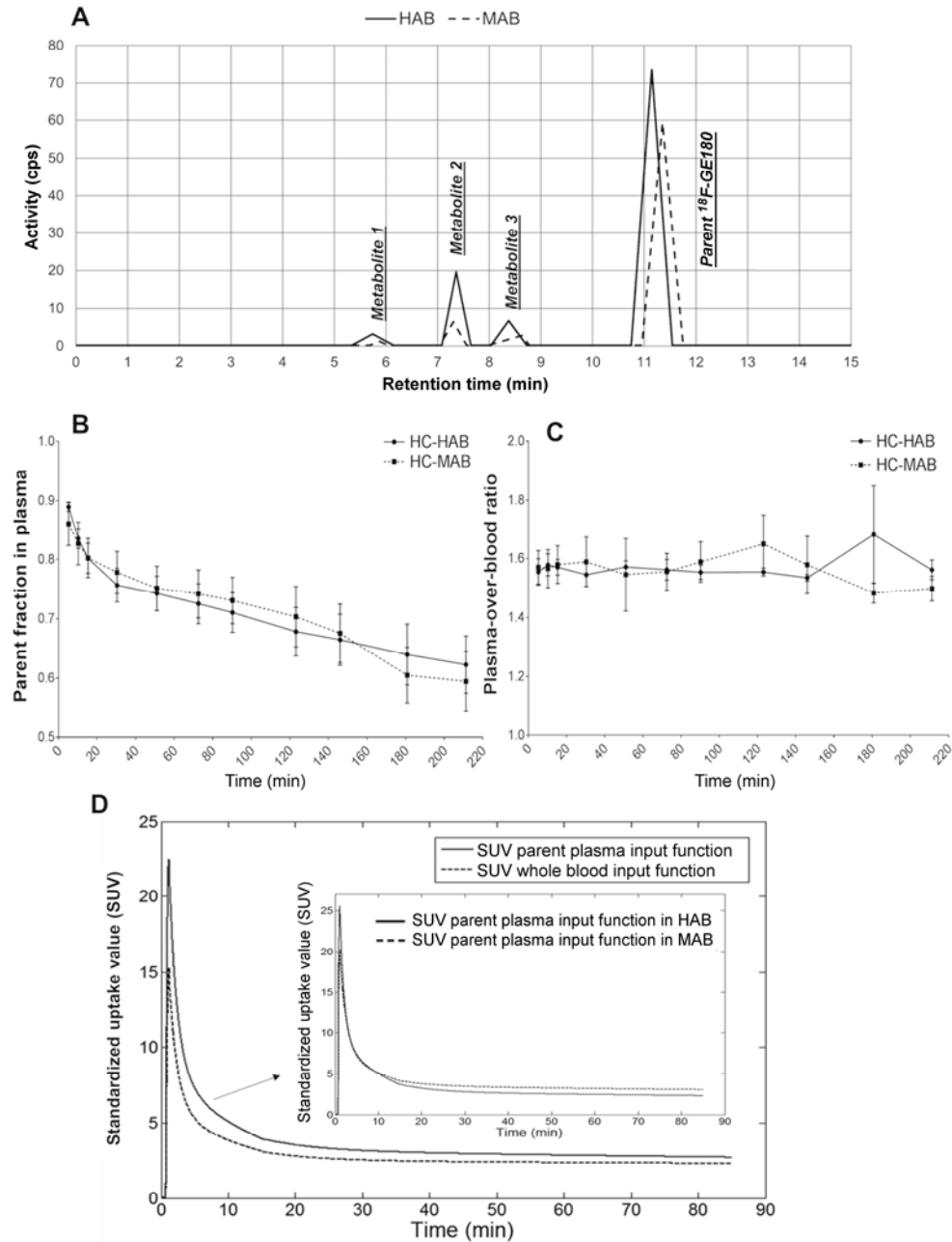


FIGURE 1. ^{18}F -GE180 blood data: (A) HPLC analysis for ^{18}F -GE180 at 15 min in a HAB subject (solid line) and a MAB subject (dashed line). (B) ^{18}F -GE180 parent fraction in arterial plasma. (C) Plasma: blood ratio in HABs (circle) and MABs (square). (D) The SUV for parent plasma and whole blood as the group and the parent plasma input function curve in either HAB or MAB cohorts.

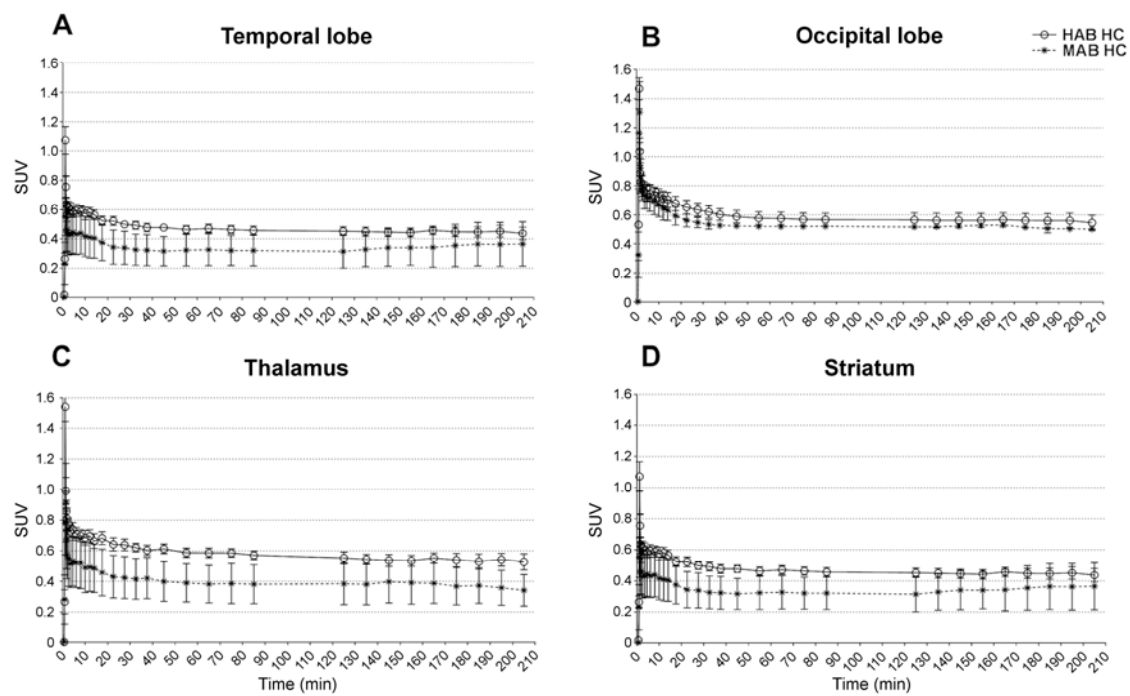


FIGURE 2. SUV corrected time-activity curves of ^{18}F -GE180 in parietal, occipital lobe, thalamus and striatum for HABs (circle) and MABs (square).

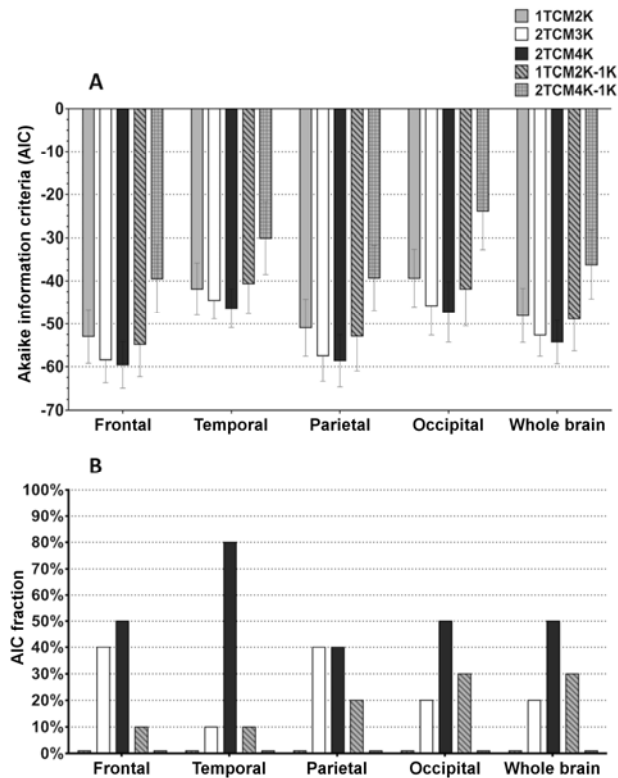


FIGURE 3. Kinetic model selection (A) This figure represents the AIC values for five models in frontal lobe, temporal lobe, parietal lobe, occipital lobe and whole brain. (B) Graph with AIC fraction, revealing the frequency of AIC preferences for each model across all subjects. Frontal = Frontal lobe, Temporal = Temporal Lobe, Parietal = Parietal Lobe, Occipital = Occipital Lobe.

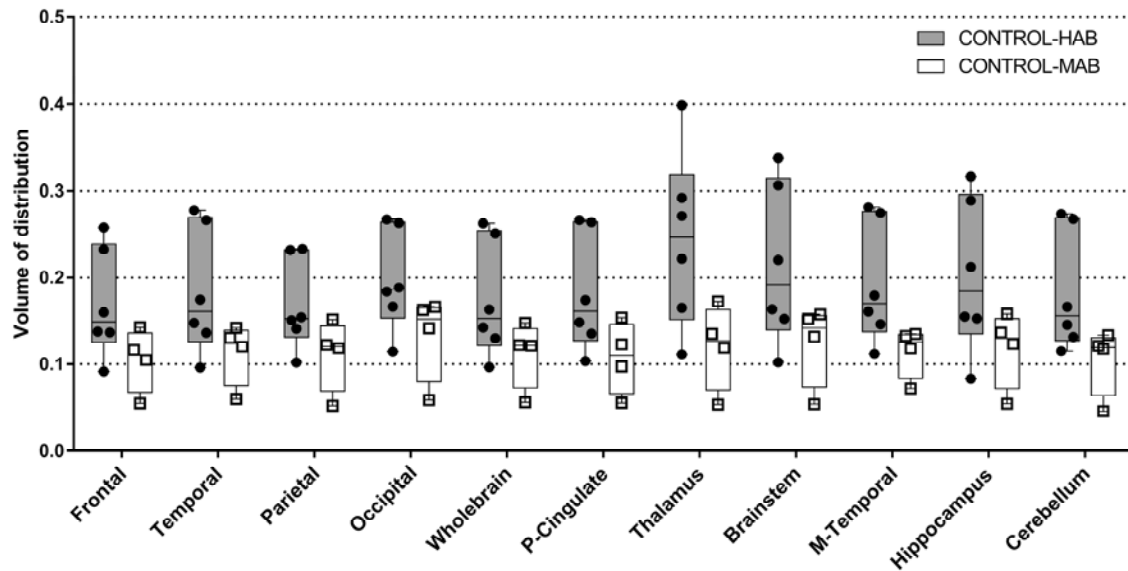


FIGURE 4. ^{18}F -GE180 regional V_T in 2TCM4k model. Regional volume of distribution with application of 2TCM4k model in twelve ROI regions. The circle with black bar represents the HABs while the square with white bar represents the MABs.

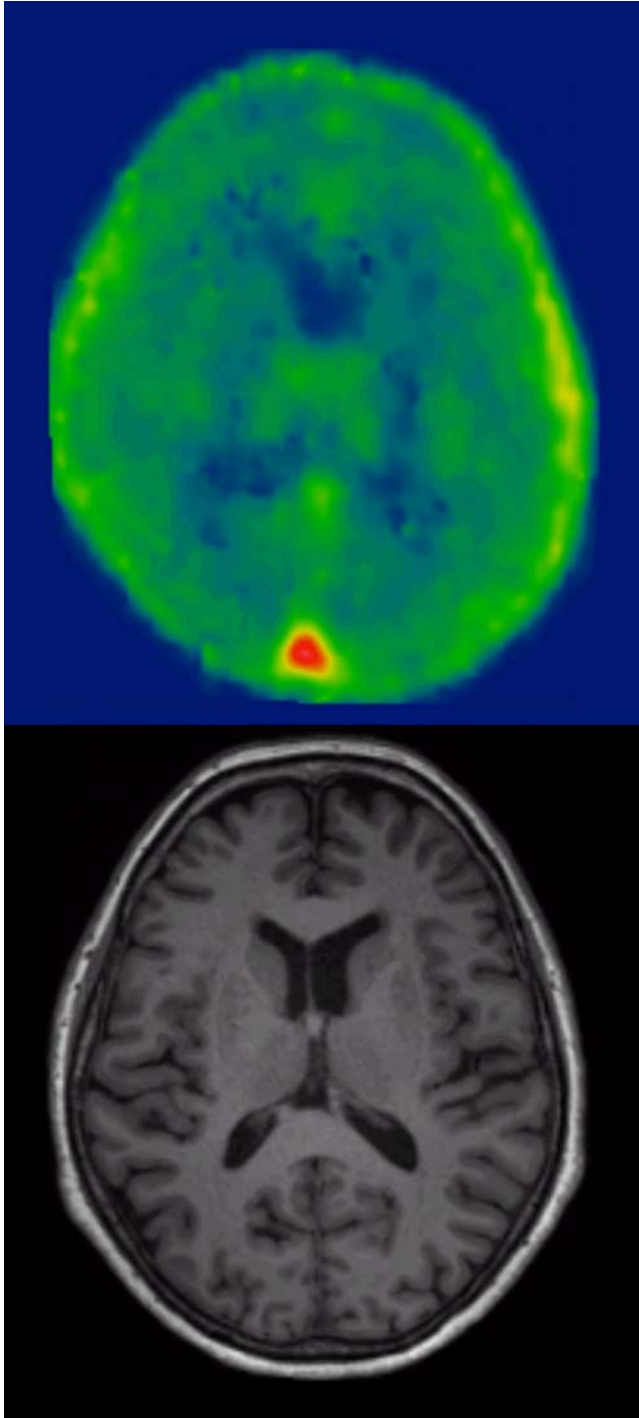


FIGURE 5. Individual ¹⁸F-GE180 Logan parametric maps in transverse view were demonstrated with its corresponding MRI.

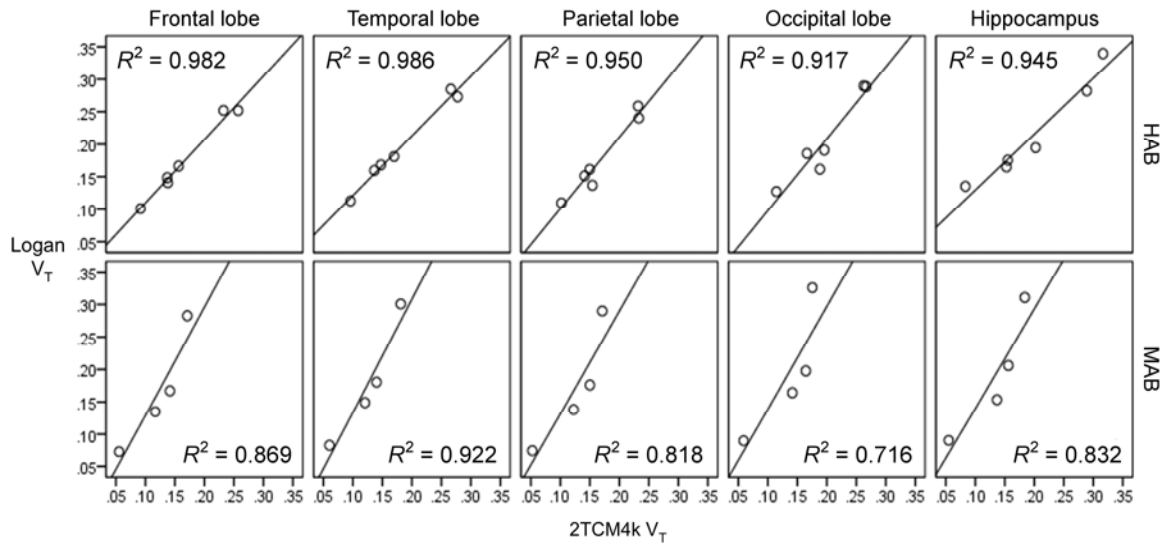


FIGURE 6. Volume of distribution in two-tissue reversible model and Logan parametric map have demonstrated similar V_T results with strong Pearson correlation in four cortices and hippocampus in both HABs ($p < 0.0001$) and MABs ($p < 0.0001$)

TABLE 1. Regional V_T for 18F-GE180 applied 2TCM4k model in all healthy controls, HABs and MABs.

18F-GE180 2TCM4K		FL	TL	PL	OL	WB	P-cing	Thalamus	Brainstem	Striatum	MTL	Hippo	CB
All Subjects	Mean	0.15	0.16	0.15	0.17	0.15	0.16	0.20	0.19	0.15	0.17	0.17	0.15
	SD	0.06	0.07	0.05	0.06	0.06	0.06	0.09	0.09	0.06	0.06	0.08	0.07
TSPO Genetic Subgroup													
HAB	Mean	0.17	0.18	0.17	0.20	0.17	0.18	0.24	0.21	0.17	0.19	0.20	0.18
	SD	0.06	0.07	0.05	0.06	0.07	0.06	0.09	0.09	0.05	0.07	0.08	0.07
MAB	Mean	0.12	0.13	0.12	0.14	0.12	0.12	0.14	0.16	0.10	0.13	0.13	0.11
	SD	0.05	0.05	0.05	0.05	0.05	0.05	0.06	0.09	0.05	0.05	0.06	0.05
HAB vs. MAB	<i>t test</i>	0.11	0.09	0.12	0.06	0.11	0.07	0.04*	0.18	0.07	0.06	0.09	0.05*
	<i>Increase</i>	39%	45%	36%	45%	40%	49%	73%	36%	64%	50%	51%	63%

* $p < 0.05$; FL = Frontal Lobe; TL = Temporal Lobe; PL = Parietal Lobe; OL = Occipital Lobe; WB = Whole Brain; P-cing = Posterior

Cingulate; MTL = Medial Temporal Lobe; Hippo = Hippocampus; and CB = Cerebellum.



The Journal of
NUCLEAR MEDICINE

Flutriciclamide (^{18}F -GE180) PET: first in human PET study of novel 3rd generation in vivo marker of human translator protein

ZHEN FAN, Valeria Calsolaro, Rebecca Ailish Atkinson, Grazia D Femminella, Adam Waldman, Christopher Buckley, William Trigg, David James Brooks, Rainer Hinz and Paul Edison

J Nucl Med.

Published online: June 3, 2016.

Doi: 10.2967/jnumed.115.169078

This article and updated information are available at:

<http://jnm.snmjournals.org/content/early/2016/06/01/jnumed.115.169078>

Information about reproducing figures, tables, or other portions of this article can be found online at:

<http://jnm.snmjournals.org/site/misc/permission.xhtml>


Information about subscriptions to JNM can be found at:

<http://jnm.snmjournals.org/site/subscriptions/online.xhtml>

JNM ahead of print articles have been peer reviewed and accepted for publication in *JNM*. They have not been copyedited, nor have they appeared in a print or online issue of the journal. Once the accepted manuscripts appear in the *JNM* ahead of print area, they will be prepared for print and online publication, which includes copyediting, typesetting, proofreading, and author review. This process may lead to differences between the accepted version of the manuscript and the final, published version.

The Journal of Nuclear Medicine is published monthly.
SNMMI | Society of Nuclear Medicine and Molecular Imaging
1850 Samuel Morse Drive, Reston, VA 20190.
(Print ISSN: 0161-5505, Online ISSN: 2159-662X)

© Copyright 2016 SNMMI; all rights reserved.

 SOCIETY OF
NUCLEAR MEDICINE
AND MOLECULAR IMAGING